Mon. Not. R. Astron. Soc. **000**, 1–9 (2015) Printed 12 November 2015 (MN LATEX style file v2.2)

# Dynamics and Metallicities of Red Supergiant Stars in the Young Massive Cluster NGC 2100

L. R. Patrick[1⋆], C. J. Evans[1,2], B. Davies[3], et al.
[1] *Institute for Astronomy, University of Edinburgh, Royal Observatory Edinburgh, Blackford Hill, Edinburgh EH9 3HJ, UK*
[2] *UK Astronomy Technology Centre, Royal Observatory Edinburgh, Blackford Hill, Edinburgh EH9 3HJ, UK*
[3] *Astrophysics Research Institute, Liverpool John Moores University, Liverpool Science Park ic2, 146 Brownlow Hill, Liverpool L3 5RF, UK*

Accepted Received 1; in original form

**ABSTRACT**
Studies of the dynamical state of young massive clusters can distinguish between models of the early time evolution of clusters. We have obtained KMOS near-IR spectroscopy for 14 red supergiant stars in the Large Magellanic Cloud (LMC) young massive star cluster NGC 2100. Radial velociteis are estiamted for the targets and the dynamical properties are estimated for the first time within this cluster. The line-of-sight velocity dispersion is shown to be flat outside of 10 pc from th cluster centre and is estimated to be $\sigma_{1D} = 3.01 \pm 0.11\,\mathrm{km\ s^{-1}}$. The dynamical mass of the cluster is derived as $log(M_{dyn}/M_{\odot}) > 4.8$ assuming virial equilibrium. Comparing this to the mass estimated using photometry we find the dynamical mass to be a factor of five smaller.

Stellar parameters including metallicity are estimated using the $J$-band analysis technique which has been rigorously tested in the Local Universe. The results of this analysis are shown to compare well with previous metallicitiy esimates within this cluster and to within the LMC in general. The age of the NGC 2100 is estimated $20 \pm 5$ Myr using isochrone fitting to the RSG population, in good agreement with previous estimates.

**Key words:** Red Supegiants: stars. Clusters: NGC 2100. Galaxy: LMC.

## 1 INTRODUCTION

Young massive clusters are important probes of cluster evolution. These custers have gained considerable attention within the past 20 years as tracers of star formation (e.g. Whitmore & Schweizer 1995; Miller et al. 1997; Zepf et al. 1999). Young massive clusters are thought to be younger counterparts to Globular Clusters. Recently, GCs have been proposed to contain multiple stellar populations based on their kinematics, metallicities and main sequence turn-offs. Studying young massive clusters can help to constrain some of the proposed models for creating multiple stellar populations within GCs.

Globular clusters (GCs) were until recently thought to consist of a simple stellar population where all of the stars within the cluster were formed from in one homogenous star forming burst. Recent results have thrown this traditional view into contention and many GCs have been shown to display an extended main-sequence turn off (ref!), double main sequences (ref!) as well as distinct chemical (Gratton et al. 2012) and dynamical(ref!) populations. The most accepted method to explain these observations is to evoke a GC with multiple stellar populations.

Niederhofer et al. (2015), show that there exists no signifanct age spread in several young massive clusters within the LMC. In recent years it has become clear that young massive clusters remain in Virial equilibrium from a young age (Longmore et al. 2014). This is in direct conflict with the formation scenario where star clusters are destroyed owing to gas explusion (i.e. infant mortality Lada & Lada 2003).

Over the last few years, medium resolution ($R > 3000$) near-IR spectroscopy has been shown to be a powerful tool to esimate stellar parameters for red supergiant stars (RSGs; Davies et al. 2010). This technique has been tested rigouroulsy in Gazak et al. (2014); Davies et al. (2015) and demonstrated with the $K$-band multi-object spectrograph first in Patrick et al. (2015) who investigate the metallicity distribution within a Local Group dwarf irregular galaxy ($d = 0.5\,Mpc$; NGC 6822) and Gazak et al. (2015) who compare the metallicity gradient derived within NGC 300, a grand design spiral galaxy outside the Local Group ($d = 1.9\,Mpc$), with that of blue supergiant stars (BSGs) and find striking agreement.

Using multi-object spectrographs like KMOS to obser

⋆ E-mail: lrp@roe.ac.uk

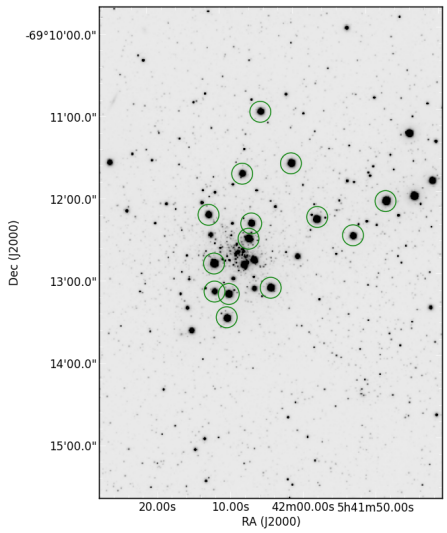


**Figure 1.** Positions of the NGC 2100 KMOS targets overlaid on a VISTA $J$-band image.

RSGs provides an efficient way to construct a sample of metallicity measurements in extragalactic stellar systems where one can study the distribution and build-up of metals within these systems.

NGC 2100 is a young massive cluster in the Large Magellanic Cloud (LMC), located near the large star forming region 30 Doradus. With an age of ∼20 Myr (Elson 1991; Niederhofer et al. 2015), and a mass of $4.6 \times 10^4 M_\odot$ (McLaughlin & van der Marel 2005, assuming King (1966) profiles) NGC 2100 falls within the mass and age range where the cluster light is dominated by RSGs (Gazak et al. 2013). This has been confirmed observationally where a large number of RSGs have been identified within this cluster.

NGC 2100 is not a cluster in isolation. This cluster is located in one of the most actively star forming regions within the Local Group of galaxies. At ∼20 Myr old, the most massive members of this star cluster have already gone supernova. This has had a profound affect on the surrounding gas and dust, and has potentially shaped the surrounding LMC 2 supershell (Points et al. 1999).

In this study we estimate stellar parameters from KMOS spectroscopy for 11 RSGs in the vicinity of the young massive cluster NGC 2100. Section 2 we describe the observations and data reduction, section 3 we detail our results, focusing on radial velocities of the target stars where we derive the line-of-sight velocity dispersion in 3.2, the dynamical mass of NGC 2100 in 3.3 and the stellar parameters in 3.4. Our results are discussed in 4 and conclusions are presented in 5.

## 2 OBSERVATIONS AND DATA REDUCTION

### 2.1 Target Selection

- Ben, could you write a few lines here?

### 2.2 KMOS Observations

These observations form part of the KMOS Gaurenteed Time Observing (PI: Evans) and were conducted in March 2015. The observations consist of $8 \times 10$ s exposures taken with the YJ grating with sky offset exposures (S) interleaved between the object (O) exposures in an O, S, O observing pattern. In addition, a standard set of KMOS calibration frames were also obtained as well as telluric standard frames using HIPXXX as the telluric standard star. Seeing conditions were stable at 1.0 arcseconds for the course of the observations.

The KMOS/esorex standard routines (Davies et al. 2013, SPARK;) were used to calibration and reconstruct the data cubes. Telluric correction was performed using the 24-arm telluric correction routine (described in detail in Patrick et al. (2015)). Briefly, corrections to the standard telluric recipe are put in place to correct for slight differences in wavelength calibration between the telluric and science spectra. This is implemented using an itertive cross-correlation approach. Additionally, differences in the strength of the telluric features are corrected by apply a simple scaling using the equation,

$$T_2 = (T_1 + c)/(1 + c) \quad (1)$$

where $T_2$ is the scaled telluric-standard spectrum, $T_1$ is the uncorrected telluric-standard spectrum and $c$ is the scaling parameter which is varied from $c = -0.5$ to $c = 0.5$ in incriments of 0.02. Once these corrections are in place, the scicence spectra are divided by the appropriate telluric spectrum for that particular IFU.

## 3 RESULTS

### 3.1 Radial velocities

Radial velocities are estimated using an iterative cross-correlation method. To ensure the KMOS spectra are at rest wavelength, the observed spectra are first cross-correlated against a model telluric spectrum, taken from the ISSAC web-pages, which is known to be at a much higher resolution than that of the observations. This cross-correlation is performed in the $1.15 - 1.17\,\mu$m region as this is where the telluric features dominate.

Once the observed spectra are at rest wavelength, an initial guess of the radial velocity is estimated by cross-correlating the science spectra with an appropriate synthetic RSG spectrum in the $1.17 - 1.21\,\mu$m region. This wavelength regime is selected based on the dominance of atomic features in the RSG spectrum at these wavelengths. To increase reliability, this initial guess is improved upon by using five carefully selected groups of stellar absorption lines centred on some of the strongest atomic features in this region. These lines and regions are selected based on their reliability and are known to be not affected by telluric absorption. Figure 2 illustrates which features have been used for the analysis.

Radial velocities are independently calculatedfor each of region by means of iterative cross-correlation. This results in five estimates of the radial velocity for each star which are then compared and any region which produces a radial velocity which is an obvious outlier to the distribution is

**Table 1.** Summary of VLT-KMOS targets in NGC 6822.

| ID | S/N | $\alpha$ (J2000) | $\delta$ (J2000) | $B$ | $V$ | $I$ | $J$ | $H$ | $K_s$ | RV (km s$^{-1}$) | Notes |
|---|---|---|---|---|---|---|---|---|---|---|---|
| 0207-0134568 | 318 | 05:41:47.873 | -69:12:05.959 | 16.488 | 13.749 | 9.769 | 9.525 | 8.603 | 8.200 | 238.9±1.1 | |
| 0207-0134683 | 198 | 05:41:52.430 | -69:12:30.410 | 16.430 | 14.267 | 11.970 | 10.413 | 9.526 | 9.155 | 238.7±2.2 | |
| 0207-0134811 | 202 | 05:41:57.286 | -69:12:16.480 | 14.074 | 13.019 | 11.170 | 9.811 | 9.036 | 8.738 | 239.8±1.3 | C2 |
| 0207-0134979 | 252 | 05:42:03.877 | -69:13:07.410 | 15.624 | 13.579 | 11.410 | 9.839 | 8.996 | 8.740 | 240.4±1.5 | |
| 0207-0135059 | 196 | 05:42:06.348 | -69:12:20.150 | 00.000 | 00.000 | 11.810 | 10.371 | 9.480 | 9.159 | 245.0±2.9 | B17 |
| 0207-0135069 | 256 | 05:42:06.764 | -69:12:31.245 | 15.643 | 13.675 | 11.390 | 9.977 | 9.150 | 8.807 | 239.5±2.3 | |
| 0207-0135150 | 240 | 05:42:09.647 | -69:13:11.263 | 15.367 | 13.383 | 11.370 | 9.976 | 9.136 | 8.841 | 240.8±3.2 | |
| 0207-0135162 | 250 | 05:42:10.001 | -69:13:28.210 | 16.060 | 13.827 | 11.580 | 10.021 | 9.150 | 8.823 | 240.2±1.4 | C32 |
| 0207-0135205 | 304 | 05:42:11.574 | -69:12:48.770 | 16.327 | 14.033 | 11.450 | 9.557 | 8.617 | 8.264 | 238.0±1.9 | |
| 0207-0135206 | 151 | 05:42:11.592 | -69:13:09.257 | 16.165 | 14.272 | 12.340 | 10.943 | 10.090 | 9.788 | 241.4±2.5 | |
| 0207-0135220 | 195 | 05:42:12.182 | -69:12:13.144 | 15.483 | 13.606 | 11.750 | 10.440 | 9.622 | 9.335 | 246.0±3.3 | |
| 0208-0135292 | 262 | 05:42:00.722 | -69:11:36.925 | 15.579 | 13.674 | 9.421 | 9.900 | 9.017 | 8.683 | 242.2±3.1 | |
| 0208-0135383 | 211 | 05:42:04.762 | -69:10:58.816 | 15.550 | 13.800 | 12.770 | 10.319 | 9.427 | 9.159 | 245.7±2.3 | |
| 0208-0135446 | 201 | 05:42:07.435 | -69:11:43.692 | 15.531 | 13.661 | 11.780 | 10.482 | 9.610 | 9.351 | 242.4±3.2 | |

Photometric data taken from the SIMBAD database. Typical errors on photometric data: 0.026, 0.014, 0.04, 0.024, 0.026, 0.022 respectively. Near-IR data taken from 2MASS.

rejected. The final radial velocity for each star is the mean of the distribution resulting from the (non-rejected) regions. The error on this mean is calculated by taking the standard deviation of the data, normalised by the number of regions used ($err = \sigma/N_{regions}$). This method is shown to work well for KMOS spectra (Lapenna et al. 2015; Patrick et al. 2015).

Figure 3 shows the radial velocities for all targets as a function of distance from the centre of the cluster, shown alongside the systemic radial velocity of the LMC (green dashed line). Here the cluster centre is defined ... (currently using SIMBAD!). Table 2 displays previous radial velocity measurements within this cluster. Recently, Evans et al. (2015) used AAOmega to measure radial velocities of massive stars within LMC, which included two sources in NGC 2100: star 407 (O9.5 II) 258.5±3.4 and star 408 (B3 Ia) 250.6 ± 1.3.

Jasniewicz & Thevenin (1994) measure radial velocities for four RSGs in NGC 2100 (B17, C2, C32 and C34 using the nomenclature of Robertson 1974). Three of these stars have been observed with KMOS in the present study (207-0135059; B17, 207-0134811; C2 and 207-0135162; C32). A comparison between the radial velocities estimated in JT94 with those presented here highlight the discrepancy between the velocites estiamted in this study. The esimates in this study are 2, 4 and 3 $\sigma$ disprepant, respectively, from the estiamtes in JT94.

Freeman et al. (1983) compile integrated light radial velocities from Andrews & Lloyd Evans (1972) and Ford (1970) to define an average of 267 ± 13 km s$^{-1}$. Whereas Smith & Weedman (1971), measure the radial velocity of the HII gas of NGC 2100 as 282.2 ± 2.5 km s$^{-1}$.

### 3.2 Velocity Dispersion

An upper limit to the line-of-sight velocity dispersion can calculated using the equations,

$$\mu = \frac{1}{\sum_i 1/\sigma_i^2} \sum_i \frac{RV_i}{\sigma_i}, \quad (2)$$

$$Var = \frac{1}{\sum_i 1/\sigma_i^2} \sum_i \frac{(RV_i - \mu)^2}{\sigma_i^2}, \quad (3)$$

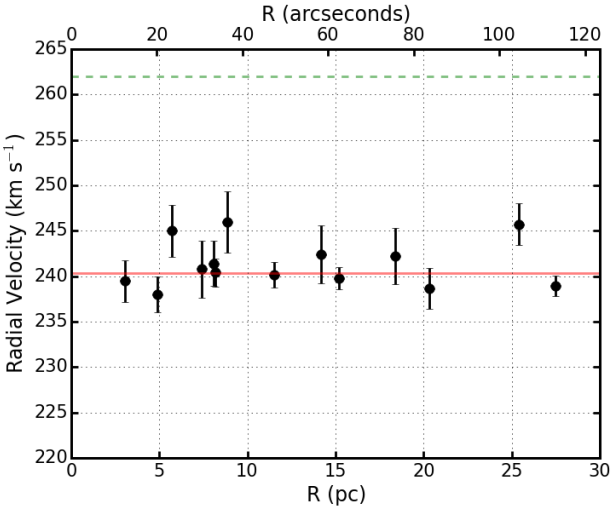


**Figure 3.** Radial velocities of KMOS targets shown as a function of distance from the cluster centre. Green dashed line shows the LMC systemtic veloctiy (262.2 ± 3.4 km s$^{-1}$; McConnachie 2012) and the solid red line shows the mean of the sample (241.3 ± 2.5 km s$^{-1}$).

$$\sigma_{1D} = \sqrt{Var \frac{N}{N-1}}, \quad (4)$$

where $\sigma_i$ is the uncertainty on the radial velocity measurement $RV_i$ and $N$ is the number of stars in the sample (Hénault-Brunet et al. 2012, and references therin). Figure 4 shows the line-of-sight velocity dispersion profile for RSGs in NGC 2100. We can see that within 10 pc the velocity dispersion increases to ∼3 km s$^{-1}$, where it appears to remain constant. This increase could be owing to the small number statistics within this radius. Thus, we adopt $\sigma_{1D}$ = 3.10±0.11 km s$^{-1}$, where the error is the average error of the radial velocities of the sample, as an upper limit on the line-of-sight velocity dispersion profile of NGC 2100. As RSGs are observationally intrinsicly single objects (REFs!!!), we do not expect this dispersion to be affected significantly by binary motions, which are known to increase the dispersion profile of young massive clusters (Gieles et al. 2010; Hénault-Brunet et al. 2012).

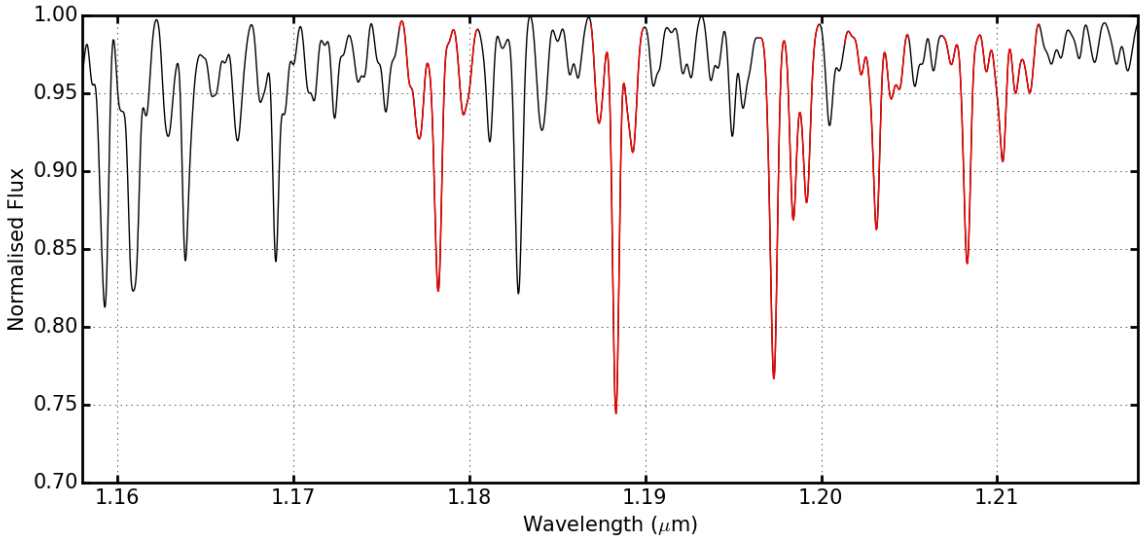


**Figure 2.** Sythetic RSG spectrum used calcualte the radial velocities for programme stars. Red regions illustrate regions where a cross-correlation is performed between the observed spectra and this synthetic spectrum. These regions provide consistent results with an average dispersion between the five regions of of 2.3 km s$^{-1}$.

**Table 2.** Previous radial velocity measurements in NGC 2100.

| ID | ID in current study | RV (km s$^{-1}$) | Reference | Notes |
|---|---|---|---|---|
| 407 | — | $258.5 \pm 3.4$ | Evans et al. (2015) | O9.5 II |
| 408 | — | $250.6 \pm 1.3$ | Evans et al. (2015) | B3 Ia |
| B17 | 207-0135059 | $255 \pm 8/245.0 \pm 2.9$ | Jasniewicz & Thevenin (1994) | |
| C2 | 207-0134811 | $270 \pm 8/239.8 \pm 1.3$ | Jasniewicz & Thevenin (1994) | |
| C32 | 207-0135162 | $260 \pm 8/240.2 \pm 1.4$ | Jasniewicz & Thevenin (1994) | |
| C34 | — | $265 \pm 8$ | Jasniewicz & Thevenin (1994) | |
| NGC 2100 | — | $280 \pm 10(16)$ | Andrews & Lloyd Evans (1972) | Whole cluster |
| NGC 2100 | — | $282.2 \pm 2.5$ | Smith & Weedman (1971) | Gas |
| NGC 2100 | — | $253 \pm 17$ | Ford (1970) | |

Value in braces is the error defined from Freeman et al. (1983).

### 3.3 Dynamical Mass

Using $\sigma_{1D}$ as an upper limit on the velocity distribution, one can calculate the dynamical/virial mass of the cluster using the equation,

$$M_{vir} = \frac{\eta \sigma_{1D}^2 r_{eff}}{G}, \quad (5)$$

where $M_{vir}$ is the virial mass, $\eta = 6r_{vir}/r_{eff} = 9.75$ providing the density profile of the cluster is sufficently steep (Portegies Zwart et al. 2010). However, NGC 2100 has a relatively shallow density profile ($\gamma = 2.3$) which means $\eta > 9.75$ therefore the estimate of $M_{vir}$ is knowingly an overestimate. Using this equation the dynamical mass of NGC 2100 is $log(M_{dyn}/M_{\odot}) = 5.0$. Comparing this to the photometric mass derived in ($log(M_{phot}/M_{\odot}) = 4.36$; McLaughlin & van der Marel 2005) we see that the dynamical mass is larger, which is expected owing to binary motions within the cluster (Gieles et al. 2010). However, the mean lifetime for RSGs within binary systems is significantly decreased (Eldridge et al. 2008). This means that it is reasonable to assume the stars in the sample are single Davies et al. (2009). Therefore, the velocity dispersion profile derived using an effectively single sample of RSGs should not be affected by binary motions. This leads to the conclusion that the only factor affecting the estimation of $M_{vir}$ is the $\eta$ parameter. Using a lower limit of $\eta = 7.0$ (estimated from Fig. 4a from Portegies Zwart et al. 2010), $log(M_{dyn}/M_{\odot}) = 4.8$ which still lies significantly (where are the errors!!!) above the photometric mass. Why this is the case is addressed in section 4.

### 3.4 Stellar Parameters

Stellar paramaeters are estimated using the J-band analysis technique descibred initially in Davies et al. (2010) and tested rigorously in Gazak et al. (2014) and Davies et al. (2015). These studies show that using a narrow spectral window within the $J$-band one can accurately derive global metallicitiy ([Z]) to within $\pm 0.2\,dex$ at the resolution of KMOS observations with S/N $\geqslant$ 100. Patrick et al. (2015) demonstrates the feasibility of this technique using KMOS spectra.

This analysis uses synthetic RSG spectra, extracted from MARCS model atmospheres (Gustafsson et al. 2008), computed with non-local thermodynamic equilibrium cor-

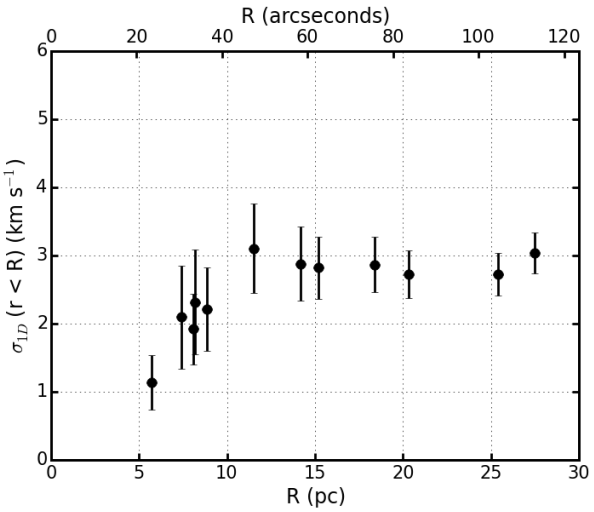


**Figure 4.** Observed line-of-sight velocity dispersion as a function of the distance from the centre of NGC 2100.

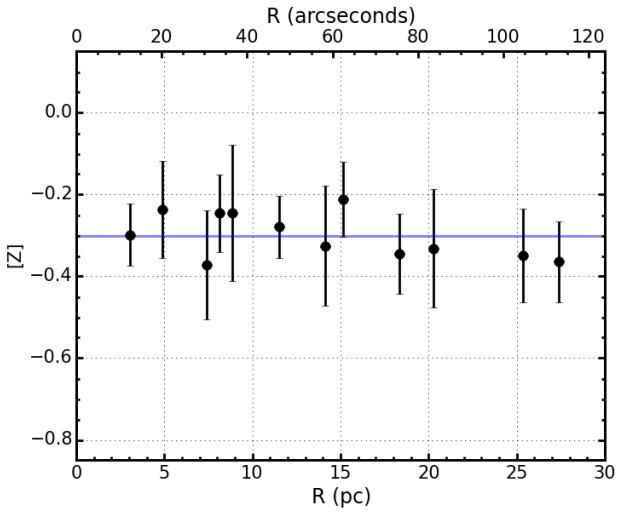


**Figure 6.** Estimated metallicities shown against distance from the centre of the cluster where the solid blue line denotes the mean of the sample $-0.3 \pm 0.11\,dex$.

**Table 3.** Model grid used for analysis.

| Model Parameter | Min. | Max. | Step size |
|---|---|---|---|
| $T_{eff}$ (K) | 3400 | 4400 | 100 |
| [Z] (dex) | −1.0 | 1.0 | 0.1 |
| $\log g$ (cgs) | −1.00 | 1.00 | 0.25 |
| $\xi$ (km s$^{-1}$) | 1.0 | 5.0 | 0.2 |

rections for stellar lines for titanium, iron, silicon and magnesium (Bergemann et al. 2012, 2013, 2015). The parameter ranges for the grid of synthetic RSG spectra are listed in table 3. These synthetic spectra are compared with observations using a $\chi$-squared minimisation apporach where the synthetic spectra are degraded to the resolution of the observations.

Estimated stellar paramters are listed in table 4. Figure 5 shows the observed KMOS spectra (black) along with the best-fitting model spectrum (red). The average metallicitiy for the 11 stars within NGC 2100 is $-0.30 \pm 0.11\,dex$. This compares well to estimates of the cluster metallicitiy using isochrone fitting to the optical colour-magnitude diagram ($-0.34\,dex$; Niederhofer et al. 2015). The only other estiamte of stellar metallicity within this cluster comes from Jasniewicz & Thevenin (1994) who esimate metallicities using optical spectroscopy of four RSGs. This study finds an average metallicity for NGC 2100 $-0.32 \pm 0.03\,dex$ which our esimate agrees well with.

Using the same analysis technique, Davies et al. (2015) estimate metallicities for nine RSGs within the LMC, finding an average value of $-0.37 \pm 0.14\,dex$ which again our estimate agrees well with.

## 4 DISCUSSION

### 4.1 Stellar Parameters

As mentioned previously, JT94 measure stellar parameters for four RSGs using optical spectroscopy. These authors measure effective temperature, $log\,g$, microturblence and metallicities for each star by comparing their spectra to a set of synthetic spectra. A method not dissimilar to out own. We find that there are three targets in common with our study: B17, C2, C32. Comparing results we find **that unbelievably, all of the targets in common have problems with their fits! (5 stars have issues with their fits, in total, and three of them are in this sample! To say more on this I need to identify why exactly these fits are perturbed.)**

When we compare the average values taken from JT94 where we find excellent agreement for all parameters apart from surface gravity where our estimates are within $2\sigma$ of the previous estimates, however, as this is not a significant outlier no further discussion will be made of this and it will suffice to say that, to within the uncertainties on average our results compare well to previous estimates.

Luminosities have been estimated using the bolometric correction in Davies et al. (2013) and a H-R diagram for the clusters is presented in Figure 7. Overlaid on this H-R diagram are SYCLIST stellar isochrones for both SMC-like (solid lines Georgy et al. 2013) and solar-like (dashed lines ) at various ages where stellar rotation is 40% of the critical velocity.

In Figure 8 we compare the estimated effective temperatures and metallicities with those derived for RSGs within the LMC (Davies et al. 2015). This figure shows that the range in metallicities and temperatues estimated in this study compares well with those derived in Davies et al. (2015).

### 4.2 Velocity Dispersion and Dynamical Mass

This study represents the first estimate of the line-of-sight velocity dispersion profile for NGC 2100. Comparing the estimated velocity dispersion of NGC 2100 with that of other young massive clusters in the Local Universe is useful to ascertain whether this cluster shares similar properties to other more well studied young massive clusters. We find the dynamical properties NGC 2100 is well matched by other

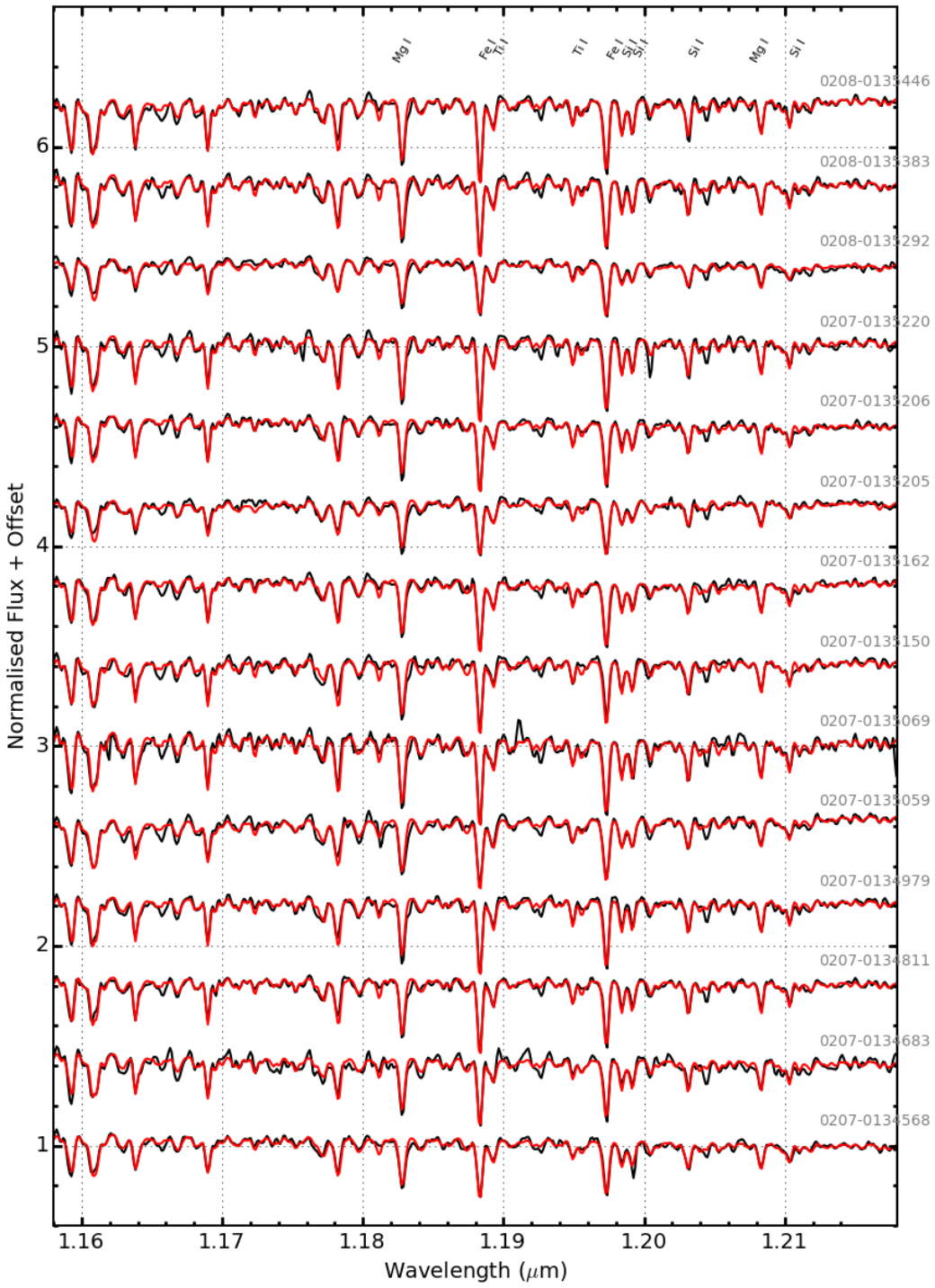


**Figure 5.** KMOS spectra of the NGC 6822 RSGs and their associated best-fit model spectra (black and red lines, respectively). The lines used for the analysis from left-to-right by species are: Fe I$\lambda\lambda$1.188285, 1.197305, Si I$\lambda\lambda$1.198419, 1.199157, 1.203151, 1.210353, Ti I$\lambda\lambda$1.189289, 1.194954.

**Table 4.** Fit parameters for NGC 2100 KMOS targets

| Target | IFU | $\xi$ (km s$^{-1}$) | [Z] | log $g$ | T$_{eff}$ (K) | Notes |
|---|---|---|---|---|---|---|
| 0207-0134568 | 7 | 3.8 ± 0.3 | -0.36 ± 0.10 | 0.50 ± 0.09 | 4017 ± 55 | |
| 0207-0134683 | 9 | 3.6 ± 0.3 | -0.33 ± 0.15 | 0.96 ± 0.38 | 4100 ± 71 | |
| 0207-0134811 | 6 | 5.0 ± 0.1 | -0.21 ± 0.09 | 0.67 ± 0.17 | 4084 ± 47 | C2 |
| 0207-0134979 | 12 | 4.4 ± 0.3 | -0.25 ± 0.10 | 0.74 ± 0.12 | 4000 ± 31 | |
| 0207-0135059 | 24 | 2.2 ± 0.8 | 0.32 ± 0.42 | 0.85 ± 0.11 | 3715 ± 181 | B17 |
| 0207-0135069 | 10 | 4.9 ± 0.1 | -0.30 ± 0.08 | 0.70 ± 0.12 | 4013 ± 37 | |
| 0207-0135150 | 14 | 4.1 ± 0.3 | -0.37 ± 0.13 | 0.73 ± 0.14 | 3900 ± 57 | |
| 0207-0135162 | 11 | 5.0 ± 0.1 | -0.28 ± 0.08 | 0.70 ± 0.19 | 4024 ± 43 | C32 |
| 0207-0135205 | 20 | 4.2 ± 0.3 | -0.24 ± 0.12 | 0.50 ± 0.09 | 3896 ± 61 | |
| 0207-0135206 | 18 | 2.0 ± 0.4 | 0.56 ± 0.23 | 1.00 ± 0.00 | 3671 ± 104 | |
| 0207-0135220 | 22 | 3.6 ± 0.4 | -0.24 ± 0.17 | 1.00 ± 0.12 | 4034 ± 50 | |
| 0208-0135292 | 4 | 4.3 ± 0.3 | -0.34 ± 0.10 | 0.75 ± 0.10 | 3947 ± 50 | |
| 0208-0135383 | 3 | 4.2 ± 0.3 | -0.35 ± 0.11 | 0.91 ± 0.16 | 3965 ± 50 | |
| 0208-0135446 | 2 | 4.1 ± 0.3 | -0.33 ± 0.15 | 0.97 ± 0.11 | 3911 ± 67 | |

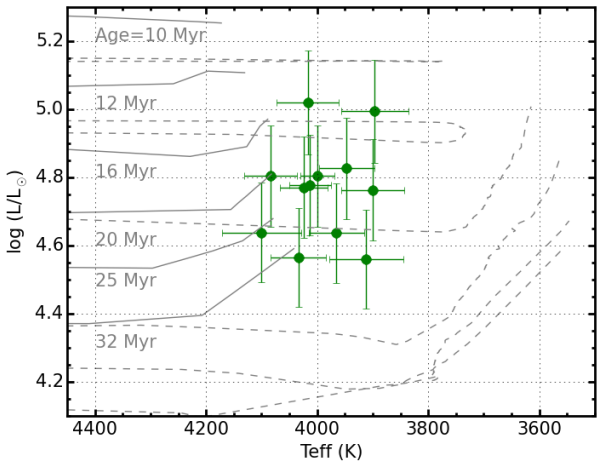


**Figure 7.** H-R diagram for 12 RSGs in NGC2100. Bolometric corrections computed using Davies et al. (2013). Cluster isochrones from Georgy et al. (2013) are overlaid in grey at a metallicity of $Z = -0.85\,dex$ without stellar rotation at ages of 10...30 Myrs.

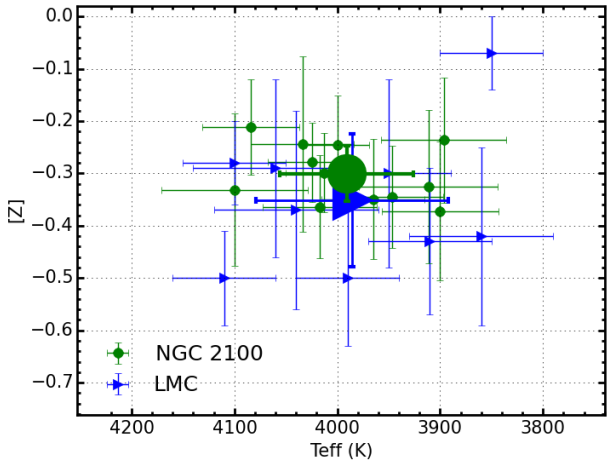


**Figure 8.** Estimated metallicities shown against estimated effective temperature.

clusters with similar masses and ages, particularly so with RSGC02, a Galactic young massive cluster. Below we compare the dynamical results for NGC 2100 to that of several young massive clusters first within the LMC and then within the Galaxy.

### *4.2.1 Comparison with LMC clusters*

The line-of-sight velocity dispersion profile of the young massive cluster R136 has been estimated at 6 km s$^{-1}$ (Hénault-Brunet et al. 2012) using multi-epoch spectroscopy from the VLT-Flames Tarantula Survey (Evans et al. 2011). NGC 2100 and R136 are both located within the 30 Doradus region and within the LMC 2 supershell. R136 is around twice as massive as NGC 2100 with the photmetric mass of R136 being estiamted at $\sim 10^5 M_\odot$ with an age less than 2 Myr (de Koter et al. 1998; Massey & Hunter 1998; Crowther et al. 2010). This makes R136 significantly younger than NGC 2100 ($\sim$ 20 Myr) and it is therefore unsurprising that the velocity dispersion profile is larger for R136 as one would expect a massive cluster to relax over time.

NGC 1850 is a young LMC massive cluster with a photometric mass of $1.4 \times 10^5$ and a recently revised age of $93\,Myr$ (Niederhofer et al. 2015). McLaughlin & van der Marel (2005) report a line-of-sight velocity dispersion for this cluster as $3.0 \pm 0.7$ km s$^{-1}$which compares well to the dispersion in NGC 2100 eventhough this cluster is significantly older are more massive.

NGC 2004 is a young massive cluster in the LMC with a mass and age similar to that of NGC 2100 (20 Myr; $2 \times 10^4 M_\odot$ Niederhofer et al. 2015, and references therein). Evans et al. (2006) obtained multi-epoch spectra for massive stars within this cluster and derive radial velocities without however dynamical anaylsis of the cluster. This cluster has remarkably similar properties to NGC 2100 and therefore a comparison between their dynamical properties is useful to the intrinsic distriubtion of dynamical properties within yound massive clusters.

### *4.2.2 Comparison with Galactic Clusters*

RSGC01 is a cluster with a large population of RSGs within the Galaxy (Davies et al. 2007). This cluster is shown to

have a mass $\sim 3 \times 10^4 M_\odot$ with an age 17 Myr and a velocity dispersion of 2.8 km s$^{-1}$. Therefore this cluster compares remarkably well with NGC 2100.

Westerlund 1 is a massive young star cluster in the Galaxy with a large population of massive stars (Clark et al. 2005). This cluster is young compared to NGC 2100 with an age of 3.5 Myr therefore many of the stars which will become RSGs in the future are currently fusing hydrogen on the main sequence. The photometric mass of Westerlund 1 is $\sim 3 \times 10^4 M_\odot$ with a measured velocity dispersion of 5.8 km s$^{-1}$. Like R136 in the LMC, Westerlund1 1 has a higher velocity dispersion and a young age.

## 5 CONCLUSIONS

Using KMOS spectra of 14 RSGs in NGC 2100 we have for the fist time estimated the dynamical properties of this young massive cluster. Radial velocities have been estimated using KMOS to a precision of $\sim 1$ km s$^{-1}$, demonstrating that this instrument can be used to study the dynamical properties of stars in external galaxies.

The line-of-sight velocity dispersion profile has been estiamted in Figure 4 and has been shown to be flat outside 10 pc from the cluster centre. A low velocity dispersion of xx.xx has been adopted and NGC 2100 has therefore been shown to be in Virial equilibrium. This adds evidence to the theory that young star clusters remain in virial equilibrium from an early age and hence expand owing to stellar evolution of a relatively slow timescales (10Myr; SPZ10). We compare the velocity dispersion profiles of other young massive clusters in the LMC and the Galaxy and find that the distribution of velocity dispersions is consistsent with this evolution. **Need to illustrate this with a Mass/Age vs sig figure.**

We also derive stellar parameters using the $J$-band analysis technique (Davies et al. 2010) for all targets within the sample and show that the estimated parameters agree well with previous studies within the LMC (Davies et al. 2015). Using temperatures from the analysis technique we construct a H-R diagram of RSGs within NGC 2100 and esimate the age of the cluster using isochrones fitting (Georgy et al. 2013) (Ekstrom12) to be $20 \pm 5$ Myr, in good agreement with previous esiamtes of this cluster (Niederhofer et al. 2015).

## ACKNOWLEDGMENTS

...

## REFERENCES

Andrews, P. J., & Lloyd Evans, T. 1972, MNRAS, 159, 445
Bergemann, M., Kudritzki, R.-P., Plez, B., et al. 2012, ApJ, 751, 156
Bergemann, M., Kudritzki, R.-P., Würl, M., et al. 2013, ApJ, 764, 115
Bergemann, M., Kudritzki, R.-P., Gazak, Z., Davies, B., & Plez, B. 2015, ApJ, 804, 113
Clark, J. S., Negueruela, I., Crowther, P. A., & Goodwin, S. P. 2005, A&A, 434, 949
Crowther, P. A., Schnurr, O., Hirschi, R., et al. 2010, MNRAS, 408, 731
Davies, B., Figer, D. F., Kudritzki, R.-P., et al. 2007, ApJ, 671, 781
Davies, B., Origlia, L., Kudritzki, R.-P., et al. 2009, ApJ, 696, 2014
Davies, B., Kudritzki, R.-P., & Figer, D. F. 2010, MNRAS, 407, 1203
Davies, B., Kudritzki, R.-P., Plez, B., et al. 2013, ApJ, 767, 3
Davies, B., Kudritzki, R.-P., Gazak, Z., et al. 2015, ApJ, 806, 21
Davies, R. I., Agudo Berbel, A., Wiezorrek, E., et al. 2013, A&A, 558, A56
de Koter, A., Heap, S. R., & Hubeny, I. 1998, ApJ, 509, 879
Eldridge, J. J., Izzard, R. G., & Tout, C. A. 2008, MNRAS, 384, 1109
Elson, R. A. W. 1991, ApJS, 76, 185
Evans, C. J., Lennon, D. J., Smartt, S. J., & Trundle, C. 2006, A&A, 456, 623
Evans, C. J., Taylor, W. D., Hénault-Brunet, V., et al. 2011, A&A, 530, A108
Evans, C. J., van Loon, J. T., Hainich, R., & Bailey, M. 2015, arXiv:1508.03490
Ford, H., 1970, PhD. Thesis, University of Wisconsin.
Freeman, K. C., Illingworth, G., & Oemler, A., Jr. 1983, ApJ, 272, 488
Gazak, J. Z., Bastian, N., Kudritzki, R.-P., et al. 2013, MNRAS, 430, L35
Gazak, J. Z., Davies, B., Kudritzki, R., Bergemann, M., & Plez, B. 2014, ApJ, 788, 58
Gazak, J. Z., Davies, B., Bastian, N., et al. 2014, ApJ, 787, 142
Gazak, J. Z., Kudritzki, R., Evans, C., et al. 2015, ApJ, 805, 182
Georgy, C., Ekström, S., Eggenberger, P., et al. 2013, A&A, 558, A103
Gieles, M., Sana, H., & Portegies Zwart, S. F. 2010, MNRAS, 402, 1750
Gratton, R. G., Lucatello, S., Carretta, E., et al. 2012, A&A, 539, A19
Gustafsson, B., Edvardsson, B., Eriksson, K., et al. 2008, A&A, 486, 951
Hénault-Brunet, V., Evans, C. J., Sana, H., et al. 2012, A&A, 546, A73
Jasniewicz, G., & Thevenin, F. 1994, A&A, 282, 717
King, I. R. 1966, AJ, 71, 64
Lada, C. J., & Lada, E. A. 2003, ARA&A, 41, 57
Lapenna, E., Origlia, L., Mucciarelli, A., et al. 2015, ApJ, 798, 23
Longmore, S. N., Kruijssen, J. M. D., Bastian, N., et al. 2014, Protostars and Planets VI, 291
Massey, P., & Hunter, D. A. 1998, ApJ, 493, 180
McConnachie, A. W. 2012, AJ, 144, 4
McLaughlin, D. E., & van der Marel, R. P. 2005, ApJS, 161, 304
Miller, B. W., Whitmore, B. C., Schweizer, F., & Fall, S. M. 1997, AJ, 114, 2381
Niederhofer, F., Hilker, M., Bastian, N., & Silva-Villa, E. 2015, A&A, 575, A62
Patrick, L. R., Evans, C. J., Davies, B., et al. 2015, ApJ,

803, 14
Points, S. D., Chu, Y. H., Kim, S., et al. 1999, ApJ, 518, 298
Portegies Zwart, S. F., McMillan, S. L. W., & Gieles, M. 2010, ARA&A, 48, 431
Robertson, J. W. 1974, A&AS, 15, 261
Smith, M. G., & Weedman, D. W. 1971, ApJ, 169, 271
Whitmore, B. C., & Schweizer, F. 1995, AJ, 109, 960
Zepf, S. E., Ashman, K. M., English, J., Freeman, K. C., & Sharples, R. M. 1999, AJ, 118, 752